

# Performance of the LHCb muon system with cosmic rays

---

M. Anelli<sup>a</sup>, R. Antunes Nobrega<sup>b</sup>, G. Auriemma<sup>bc</sup>, W. Baldini<sup>d</sup>, G. Bencivenni<sup>a</sup>, R. Berutti<sup>ef</sup>, V. Bocci<sup>b</sup>, N. Bondar<sup>g</sup>, W. Bonivento<sup>e\*</sup>, B. Botchin<sup>g</sup>, S. Cadeddu<sup>e</sup>, P. Campana<sup>a</sup>, G. Carboni<sup>hj</sup>, A. Cardini<sup>e</sup>, M. Carletti<sup>a</sup>, P. Ciambone<sup>a</sup>, E. Dane<sup>a</sup>, S. De Capua<sup>hu</sup>, C. Deplano<sup>e</sup>, P. De Simone<sup>a</sup>, F. Dettori<sup>ef</sup>, A. Falabella<sup>di</sup>, F. Ferreira Rodriguez<sup>k</sup>, M. Frosini<sup>lm</sup>, S. Furcas<sup>an</sup>, G. Graziani<sup>l</sup>, L. Gruber<sup>op</sup>, A. Kashchuk<sup>g</sup>, A. Lai<sup>e</sup>, G. Lanfranchi<sup>a</sup>, M. Lenzi<sup>l</sup>, O. Levitskaya<sup>g</sup>, K. Mair<sup>o</sup>, O. Maev<sup>g</sup>, G. Manca<sup>e</sup>, G. Martellotti<sup>b</sup>, A. Massafferri Rodrigues<sup>jq</sup>, R. Messi<sup>hj</sup>, F. Murtas<sup>a</sup>, P. Neustroev<sup>g</sup>, R.G.C. Oldeman<sup>ef</sup>, M. Palutan<sup>a</sup>, G. Passaleva<sup>l</sup>, G. Penso<sup>br</sup>, A. Petrella<sup>di</sup>, D. Pinci<sup>b</sup>, S. Pozzi<sup>dl</sup>, G. Sabatino<sup>hj</sup>, B. Saitta<sup>ef</sup>, R. Santacesaria<sup>b</sup>, E. Santovetti<sup>hj</sup>, A. Saputi<sup>a</sup>, A. Sarti<sup>a</sup>, C. Satriano<sup>bc</sup>, A. Satta<sup>h</sup>, M. Savrié<sup>di</sup>, B. Schmidt<sup>o</sup>, T. Schneider<sup>o</sup>, A. Sciubba<sup>ar</sup>, P. Shatalov<sup>s</sup>, S. Vecchi<sup>d</sup>, M. Veltri<sup>lt</sup>, S. Volkov<sup>g</sup>, A. Vorobyev<sup>g</sup>

<sup>a</sup>Laboratori Nazionali di Frascati dell'INFN, Frascati, Italy

<sup>b</sup>Sezione INFN, Roma, Italy

<sup>c</sup>University of Basilicata, Potenza

<sup>d</sup>Sezione INFN, Ferrara, Italy

<sup>e</sup>Sezione INFN, Cagliari, Italy

<sup>f</sup>Università di Cagliari, Cagliari, Italy

<sup>g</sup>Petersburg Nuclear Physics Institute, Gatchina, St-Petersburg, Russia

<sup>h</sup>Sezione INFN, Roma Tor Vergata, Italy

<sup>i</sup>Università di Ferrara, Ferrara, Italy

<sup>j</sup>Università di Roma Tor Vergata

<sup>k</sup>Instituto de Física - Universidade Federal do Rio de Janeiro (IF-UFRJ), Rio de Janeiro, Brazil

<sup>l</sup>Sezione INFN, Firenze, Italy

<sup>m</sup>Università di Firenze, Firenze, Italy

<sup>n</sup>now at Sezione INFN, Milano, Italy

<sup>o</sup>European Organisation for Nuclear Research (CERN), Geneva, Switzerland

<sup>p</sup>Technische Universität Wien, Austria

<sup>q</sup>Centro Brasileiro de Pesquisas Físicas (CBPF), Rio de Janeiro, Brazil

<sup>r</sup>Università di Roma "La Sapienza"

<sup>s</sup>ITEP Moscow

<sup>t</sup>Università di Urbino, Urbino, Italy

<sup>u</sup>now at EPFL, Lausanne, Switzerland

**ABSTRACT:** The LHCb Muon system performance is presented using cosmic ray events collected in 2009. These events allowed to test and optimize the detector configuration before the LHC start. The space and time alignment and the measurement of chamber efficiency, time resolution and cluster size are described in detail. The results are in agreement with the expected detector performance.

**KEYWORDS:** Muon spectrometers; Trigger detectors; Wire chambers.

---

\*Corresponding author. EMail: [Walter.Bonivento@cern.ch](mailto:Walter.Bonivento@cern.ch)

---

## Contents

<b>1. Introduction</b>	<b>1</b>
<b>2. The LHCb muon system</b>	<b>2</b>
<b>3. Detector settings</b>	<b>7</b>
<b>4. Data sample and track reconstruction</b>	<b>8</b>
<b>5. Space and time alignment</b>	<b>10</b>
5.1 Space alignment	10
5.1.1 Mechanical alignment	11
5.1.2 Space alignment using tracks	11
5.2 Time alignment	13
5.2.1 Pulser time alignment of the readout chain	13
5.2.2 Time alignment using cosmic rays	14
<b>6. Detector performance</b>	<b>15</b>
6.1 Total efficiency	15
6.2 Cluster size	16
6.3 Time resolution	19
<b>7. Conclusions</b>	<b>22</b>
<b>8. Acknowledgments</b>	<b>23</b>

---

## 1. Introduction

The main purpose of the LHCb muon detector [1] is to provide the LHCb experiment with a trigger for b-hadron decay channels containing muons in the final state. Moreover, it is the main sub-detector providing off-line muon identification. It consists of five stations, M1 to M5, equipped with multi-wire proportional chambers (MWPC), with the exception of the inner part of the first station equipped with triple-GEM detectors. For triggering, the detector has to be highly efficient, more than 95 %, on muons within a time window smaller than 25ns to unambiguously identify the LHC bunch crossing. The detector and its associated readout electronics were optimized for this goal and test beams measurements with prototype detectors confirmed the expected performance. However, the construction of a very large system (1380 chambers with 122,000 readout channels), assembled in different productions sites during several years, and with some technical details different from site to site, is such that some chamber to chamber non-uniformity can be expected.

In addition, the operation of this very large system can be affected by problems not present when testing one chamber at the time in the lab or with test beams. Therefore, it is crucial to assess the system performance as a whole in order to confirm the expected results.

At the beginning of 2009 a large data sample of cosmic rays was collected. Data were taken in different detector conditions and a recursive optimization process lead to a long data taking period whose results are described in this paper.

The main optimization issues concerned the space and the time alignment. The forward geometry of the LHCb experiment is not optimal to detect cosmic rays. In particular the inner regions of the muon detector would require high statistics of almost horizontal tracks. On the other hand, cosmic rays permit a good calibration in the outer regions where muons from LHC interactions are scarce. In order to assess the system performance, the measurement of chamber efficiency, time resolution and cluster size are also described here. As the main goal of this work was to assess the performance of the detector chambers, methods have been devised to separate contributions to the efficiencies and resolutions measured with cosmic rays that are linked to the geometry of the system from contributions coming from the detector performance itself.

## 2. The LHCb muon system

LHCb [1] is an experiment dedicated to heavy flavour physics at the LHC. Its primary goal is to look for indirect evidence of new physics in CP violation and rare decays of beauty and charm hadrons. The LHCb apparatus is a single-arm forward spectrometer, consisting of a series of sub-detector systems, aligned as in a fixed-target geometry, along the beam axis. It includes a silicon-strip Vertex Locator (VELO) centered on the interaction point for precise vertex reconstruction. A dipole warm magnet provides the bending for momentum measurement. Tracking is insured by tracking stations using silicon strips (TT,IT) and straw tubes (OT) before and after the dipole. Particle identification is provided by two RICH detectors, by an electromagnetic and hadron calorimeter system (ECAL and HCAL) and by the Muon Detector.

The muon system is composed of five stations (M1-M5) of rectangular shape, placed along the beam axis. As shown in figure 1, stations M2 to M5 are placed downstream the calorimeters and are interleaved with iron absorbers 80 cm thick to select penetrating muons. Station M1 is instead located in front of the calorimeters and is used to improve the transverse momentum measurement in the first level hardware trigger L0.

The geometry of the muon detector was designed in order to fulfill requirements of both performance and easy access to the detector itself. On each station, 276 chambers are mounted on aluminium supporting walls at four different distances ( $\pm 58.5$  mm and  $\pm 142.5$  mm from the station middle plane) in order to provide with their sensitive area a hermetic geometric acceptance to high momentum particles coming from the interaction point. In addition, the chambers of different stations are placed so that they form projective towers pointing the interaction point. Each station consists of two mechanically independent halves (called A and C side), hanging from a common rail, that can be opened to access the beam pipe and the detector chambers for maintenance.

The detectors provide space point measurements of the tracks, providing binary (yes/no) information to the trigger processor and to the data acquisition (DAQ). The information is obtained by partitioning the detector into rectangular logical pads whose dimensions define the  $x$ ,  $y$  resolution.

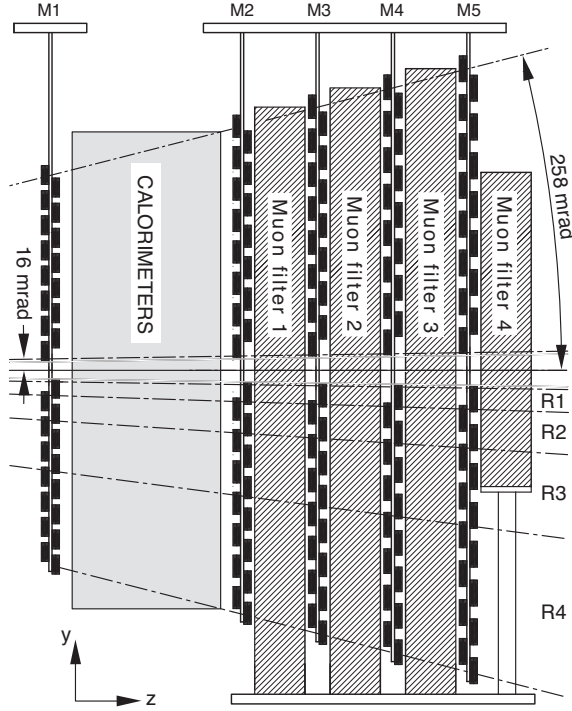


**Figure 1.** Side view of the LHCb muon system. The LHCb reference system is a right-handed coordinate system with the nominal collision point at the origin, with the  $z$  axis defined by the beam axis and directed from the VELO to the muon system.

The muon trigger is based on stand-alone muon track reconstruction and transverse momentum ( $p_T$ ) measurement, with a 20% resolution, and requires aligned hits in all five stations. Since the spectrometer dipole provides bending in the horizontal plane, the pad segmentation of muon chambers is finer in the horizontal direction than in vertical one, to allow a precise estimate of the momentum. Stations M1 to M3 are used to define the track direction and to calculate the  $p_T$  of the candidate muon and therefore have a higher spatial resolution along the  $x$  coordinate (bending plane) than stations M4 and M5, whose main purpose is the identification of penetrating particles. The dimensions of the M1 pads in the inner region of M1 station are 1 cm in  $x$  and 2.5 cm in  $y$ . The pad vertical size is the same (apart from the projective increase) in all the other stations, while the  $x$  size is two times smaller in station M2 and M3 and two times larger in M4 and M5.

The positioning of the chambers in the  $x$ - $y$  plane within a station is done in such a way as to preserve as much as possible the full projectivity of the logical layout. This is mandatory for a correct execution of the L0-muon trigger algorithm and to minimise the geometrical cluster size and geometrical inefficiencies at the boundary of the chambers. The logical layout is defined at the central plane of the station and the sensitive area of each chamber is sized as if it were at this plane. The  $x$  and  $y$  positions of the centres of each chamber within a station are obtained simply by positioning each chamber centre so that it projects from the interaction point to its position in the logical layout at the central plane of the station. In doing so, the chambers in front of the supporting wall will overlap in  $x$  with their neighbours. The overlap however is always less than half of one logical channel. Similarly, the holes introduced between the chambers located behind the supporting wall

are small, and are further limited by the thickness of the chambers in  $z$ . Viewed from the interaction point the total loss in angular acceptance is less than 0.1%. The corresponding  $y$  overlaps are negligible due to the small  $y$  dimensions of the chambers.

Each muon station is divided into four regions, R1 to R4 with increasing distance from the beam axis. The linear dimensions of the regions R1, R2, R3, R4, and their segmentation scale in the ratio 1:2:4:8, as shown in figure 2. With this geometry, the particle flux and channel occupancy are expected to be roughly of the same order of magnitude over the four regions of a given station.

The trigger algorithm requires a five-fold coincidence between all the stations, therefore the effi-

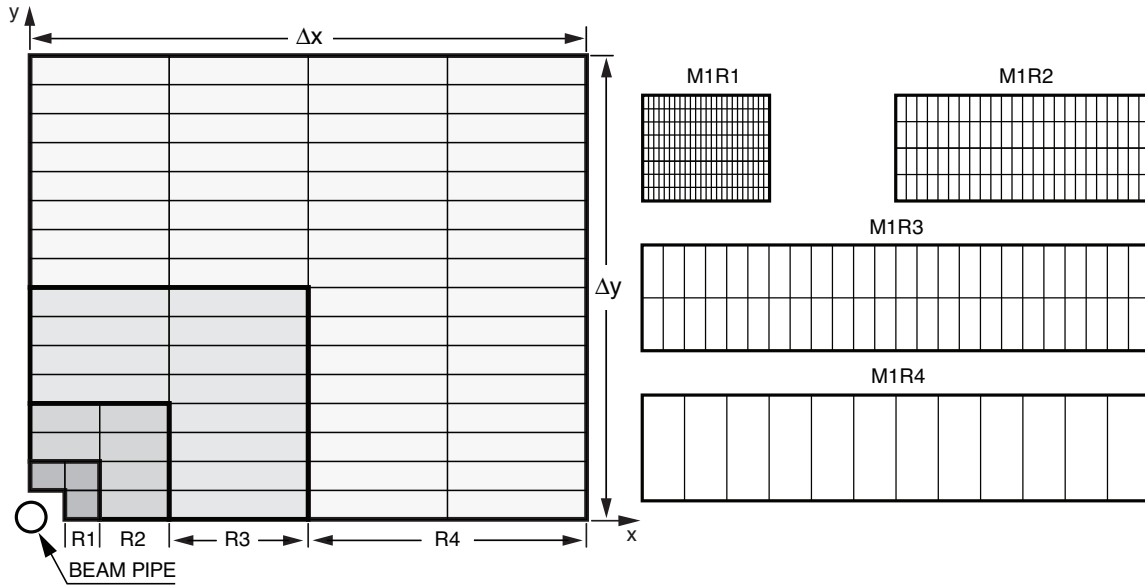


**Figure 2.** Left: front view of a quadrant of a muon station. Each rectangle represents one chamber. Each station contains 276 chambers. Right: division into logical pads of four chambers belonging to the four regions of station M1. In each region of stations M2-M3 (M4-M5) the number of pad columns per chamber is double (half) the number in the corresponding region of station M1, while the number of pad rows per chamber is the same.

ciency of each station must be  $\geq 99\%$  to obtain a trigger efficiency of at least 95%, within a time window smaller than 25 ns in order to unambiguously identify the bunch crossing (BX).

The necessary time resolution is ensured by a fast gas mixture,  $\text{Ar}/\text{CO}_2/\text{CF}_4$  40/55/5, and an optimized charge-collection geometry both for the MWPC and the GEM detectors. Moreover, the chambers are composed of four or two OR-ed gas gaps depending on station. In stations M2 to M5 the MWPC's are composed of four gas gaps arranged in two sensitive layers with independent readout, as shown in figure 3. In station M1, R2 to R4 the MWPC have only two gas gaps to minimize the material in front of the electromagnetic calorimeter. In region M1R1 two superimposed GEM chambers connected in OR are used.

Since spatial resolution and rate capability vary strongly over the detectors, different readout techniques are employed for the MWPC in different stations and regions. All the chambers are segmented into physical pads: anode wire pads, where the pads are formed by adding the analog signals coming from a certain number of adjacent wires, or cathode pads, with a segmented cathode

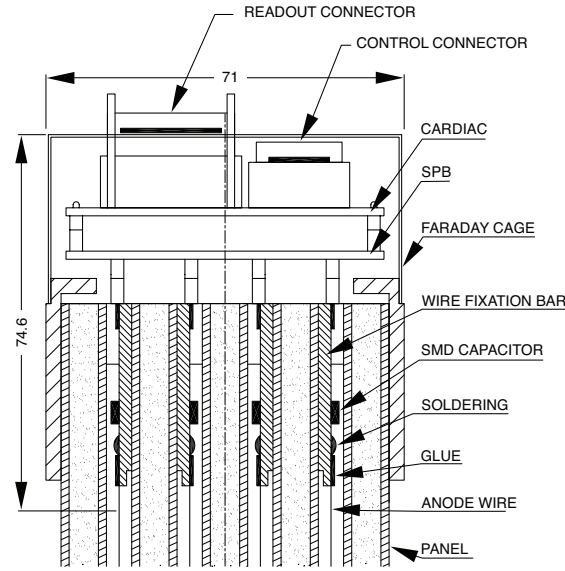


**Figure 3.** Cross section of a wire chamber showing the four gas gaps and the connection to the readout electronics. SPB: Spark Protection Board; CARDIAC: FE Electronics Board. In this case the hardwired OR forming the two double gaps (see text) is achieved in the SPB.

printed circuit board, in the MWPCs and anode pads, again with a segmented printed circuit board, in the GEM chambers.

Each physical pad is read out by one front-end (FE) electronics channel. The electronics includes flexible logical units performing the OR of a variable number of FE channels following the requirements of the readout. Up to four adjacent physical pads are OR-ed by the FE electronics to build a logical pad. In the M1 station, where the foreseen channel occupancy is high, the signals from the logical pads are sent directly to the trigger and DAQ. In most of the other regions, M2/3 R3/4 and M4/5 R2/3/4, several contiguous logical pads are further OR-ed to build larger logical channels in the form of vertical and horizontal strips. The logical pads are then reconstructed by the coincidence of two crossing strips, as shown in figure4. However, in the high granularity regions R1-R2 of stations M2-M3 a mixed readout was adopted: a narrow wire-strip defining the  $x$  resolution and a larger cathode pad defining the  $y$  resolution are the logical channels sent to the trigger and DAQ. Logical pads are then obtained as an AND between wire and cathode pads.

Figure 5 shows schematically the architecture of the Muon readout electronics. The task of the electronics is twofold: to prepare the information needed by the Level-0 muon trigger and to send the data to the DAQ system. The front-end (FE) CARDIAC boards house two eight channel ASIC's, each one containing a high bandwidth current amplifier, a shaper and a single threshold fast discriminator in leading edge mode, processing the 122 k physical signals from the chambers (CARIOCA [2]) and generate the 26 k logical-channel signals by suitable logical OR's of the physical channels (DIALOG [3]). This last step is in fact fully performed on the FE boards only in part of the detector and it is ended on special Intermediate Boards (IB) in regions where the logical channel spans more than one FE board. Eventually, the Off Detector Electronics (ODE) boards receive the signals from the logical channels. They are tagged with the number of the bunch

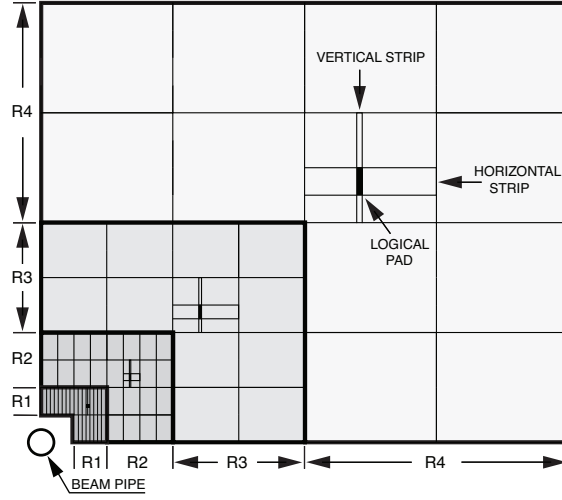


**Figure 4.** Front view of one quadrant of stations M2 and M3 showing the partitioning into sectors. In one sector of each region a horizontal and a vertical strip are shown. The intersection of a horizontal and a vertical strip defines a logical pad (see text). A Sector of region R1 (R2, R3, R4) contains 8 (4, 4, 4) horizontal strips and 6 (12, 24, 24) vertical strips.

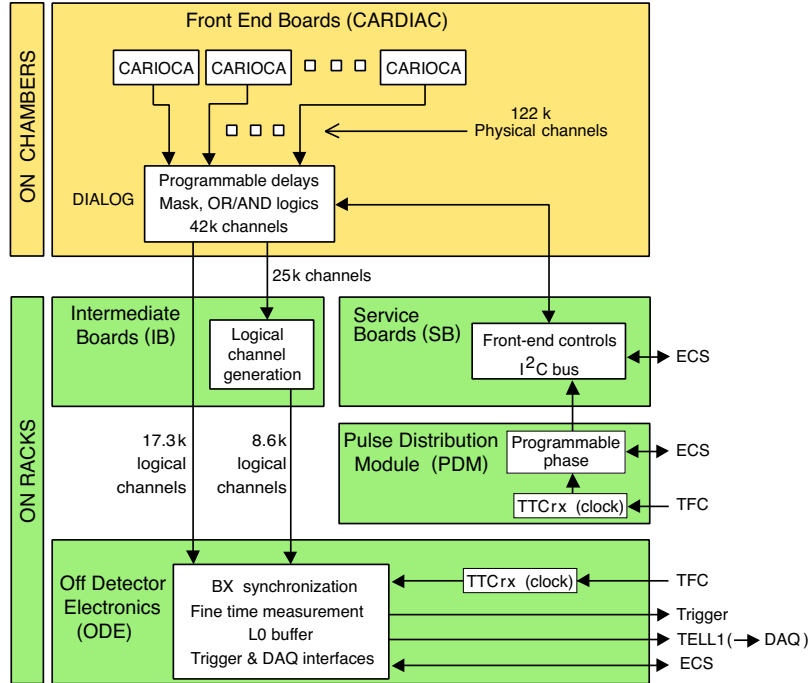


**Figure 5.** Simplified scheme of the Muon electronics architecture.

crossing (BXID) and routed to the trigger processors via optical links without zero suppression. The fine time information inside the 25 ns gate, measured by a 4-bit TDC ASIC (SYNC [4]) on the ODE boards, is added and the data are transmitted via optical links to the TELL1 board [5] and from the TELL1 to the DAQ system.



### 3. Detector settings

As described in section 2, the trigger requires the coincidence within the 25 ns LHC gate of signals from the five stations. As a safety margin, the requirement of 95 % efficiency (99 % per station) was specified in a 20 ns window. Moreover, for an optimal trigger performance, the cluster size, i.e. the average number of pads yielding a signal per track in a given chamber, should not exceed 1.3-1.4 in stations M1 to M3.

Despite the different type of readout (wire or pad), from the point of view of performance the main difference is the value of the readout pad capacitance to ground, which ranges from 50 pF to 245 pF, and affects the front-end amplifier sensitivity. The gas gaps and the wire pitch and radius are everywhere the same (except for the triple-GEM detectors) and therefore the induced charge on the electrodes is also everywhere the same, at given high voltage. In terms of detector performance, the muon detector has a crucial dependence on the gas gain to threshold ratio, since the higher this ratio the better the time resolution (and efficiency), due to the reduction of the time walk effect. Unfortunately, a higher ratio also implies higher cluster size, higher collected charge at the anodes and related aging and detector instability, such as the discharge probability, leading in the long run to detector failures. Therefore the performance optimization is a very delicate and careful work which has to take into account all these parameters.

The 20 ns detector efficiency is the main parameter qualifying chamber response in the LHCb muon system. However, this could not directly be measured with cosmic rays, due to a non linear behavior of the TDC, which will be discussed in section 5.2.2. Indeed, since the cosmic rays are not in time with the LHC clock, to measure the 20 ns detector efficiency one would have had to precisely measure the fine time all along the LHC gate, including the borders, for all hits associated to the track. Unfortunately the above mentioned TDC feature prevented us from precise measurement right at the LHC gate borders, compromising this measurement.

However, the 20 ns efficiency could be determined in an indirect way by measuring the total efficiency in an infinite time window, the chamber time resolution and using results from laboratory tests [6] to make the connection between time resolution and 20 ns detector efficiency. For comparison a chamber simulation was also performed using the drift chamber simulation program GARFIELD [7] for the gas mixture in use and a high voltage of 2.65 kV, corresponding to a gas gain of  $10^5$ . Figure 6 the 20 ns efficiency vs. time resolution obtained by simulation of four-gap chambers and two-gap chambers as well as test beam data for a M3R3 (pad readout) chamber and a M5R4 (wire readout) chamber.

To preserve long term operation of the system, the MWPC's of the LHCb muon system should be operated at the lowest possible threshold compatible with electronic noise. For the cosmic ray data taking, the thresholds were set higher than foreseen for the LHCb run at nominal luminosity in order to keep the noise level below 100 Hz per channel. The relatively large range of detector capacitance, together with the corresponding slewing effect in the front-end amplifier, is such that the same noise level is reached at quite different values of threshold if expressed in charge units. The set thresholds ranged from 2.8 fC to about 11 fC depending on stations and regions of the detector.

To equalize the gas gain to threshold ratio and therefore have the same efficiency everywhere no matter what the detector capacitance is, different high voltage values in each individual region and

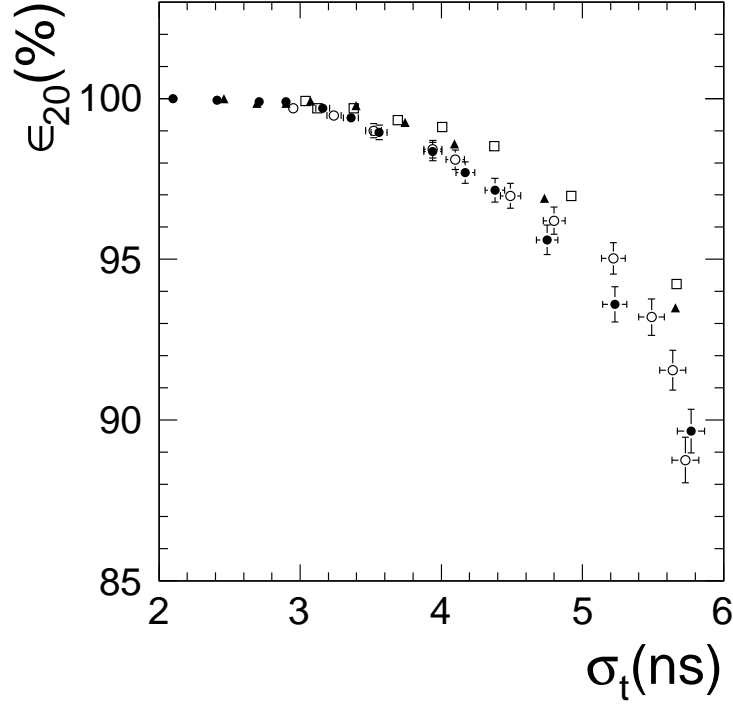


**Figure 6.** Efficiency in 20 ns vs. time resolution (c) from a simulation of four-gap chambers (solid circles) and two-gap chambers (open circles) and test beam data for a M3R3 (pad readout) chamber (solid triangles) and a M5R4 (wire readout) chamber (open squares).

station [8] would have to be set. However, for the cosmic ray acquisition runs and the first very low luminosity LHC run, it was decided to start with the same value of the high voltage, 2.65 kV, for the whole detector, set to the highest calculated value among the different regions and stations compatible with the efficiency requirements and with detector stability. Therefore, this high voltage settings leads in some stations and regions to a larger than needed ratio of high voltage to threshold, i.e. to an expected 20 ns efficiency beyond 99%. A more careful tuning of this ratio will be performed in the future. Figure 7 shows the noise rate for the whole muon system after threshold setting and shows that for 99.3 % of all the channels the noise is below 100 Hz and that for 99.8 % of the channels the noise rate is below 1 kHz.

#### 4. Data sample and track reconstruction

The data sample for the analysis described in this paper consisted of 2.5 million cosmic ray events triggered by the calorimeter, with the threshold set to detect minimum ionizing particles. Events were acquired, according to a prescription of the DAQ team which affected all LHCb sub-detectors, in a time window of five LHC gates, i.e. 125 ns (*wide gate* in the following). This wide gate indeed proved to be very useful since it allowed track reconstruction and a quite detailed study of the time

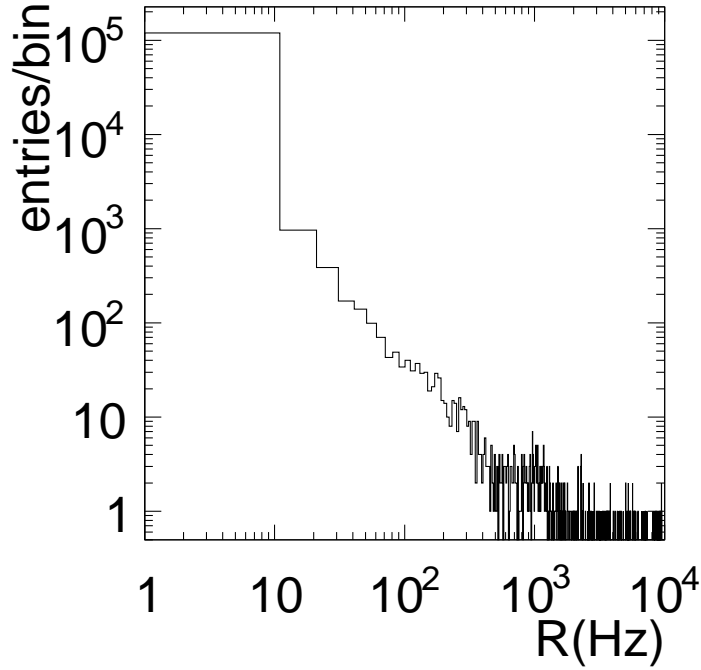


**Figure 7.** Measured noise rate  $R(\text{Hz})$  for all channels of the muon system.

properties of signals, including cross-talk, even before a precise time alignment of the detector took place.

Even if the LHCb geometry is not optimal for cosmic ray detection, the calorimeter trigger provided events at the rate of few Hz.

The LHCb standard pattern recognition and tracking rely heavily on the position of the primary interaction vertex, and this makes it unsuitable to reconstruct cosmic ray tracks. Therefore two ad-hoc stand-alone pattern recognition methods were developed. For space and time alignment, time resolution and efficiency studies, a neural network approach [9] was used, which is highly efficient and also allowed the reconstruction of multiple tracks per trigger. Pattern recognition started from clusters of adjacent pads and the hit position in a station was determined from the cluster barycenter. For cluster size and for a second analysis of the total efficiency, a standard pattern recognition algorithm was used, looking for the combination of more than three aligned hits (one per station) providing the best fit, taking into account multiple scattering effects in the iron wall and in the calorimeters. In both cases the fit tracks were straight lines, given that no magnetic field was present in the muon chambers.

With the neural network approach, about 250,000 tracks were reconstructed with at least four hit stations. Figure 8 shows the track angles  $\theta_{xz}$ , in the  $xz$  plane, (a) and  $\theta_{yz}$ , in the  $yz$  plane, (b), in the LHCb reference frame; the two peaks at negative and positive  $\theta_{yz}$  in figure 8(b) correspond to cosmic rays going forward and backward in the apparatus.

As seen from figure 8, cosmic rays have a very different spatial and angular distributions compared

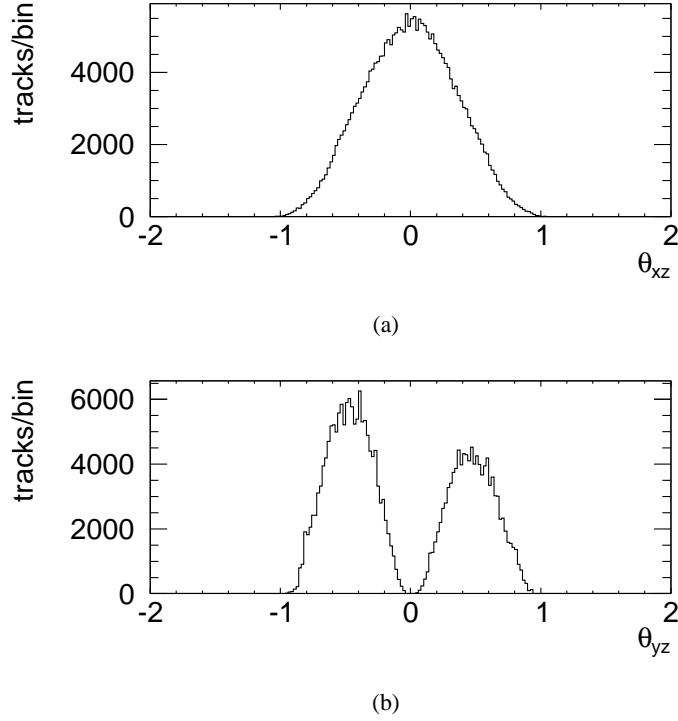


**Figure 8.** Angles (rad) in the horizontal plane  $\theta_{xz}$  (a) and in the vertical plane  $\theta_{yz}$  (b) in the LHCb reference frame for reconstructed cosmic ray tracks.

to particles coming from the interaction point. The muon detector is indeed built to be hermetic for tracks in acceptance coming from the interaction point by a suitable layout of the chambers in the stations. For this reason, cosmic rays can go through un-instrumented areas of the detector, yielding a strong angular dependence of the efficiency, which in turn leads to potential systematic effects in the total efficiency determination and in the space alignment procedure, which should be carefully studied.

## 5. Space and time alignment

Two essential ingredients to optimize the system performance are the space and time alignment, which are described hereafter and have to be performed before the efficiency and the resolution measurements.

### 5.1 Space alignment

The accurate spatial alignment of the muon detector is important to guarantee the design performance of trigger and off line muon identification. Given the spatial resolution of the detector readout elements, the needed alignment accuracy is driven by the trigger requirements in the inner regions of stations M1, M2 and M3. A precision of  $\sim 1$  mm in  $x$  and  $y$  directions is sufficient to guarantee the design specifications. The alignment requirements along  $z$  are much less demanding due to the forward geometry of the experiment.

### 5.1.1 Mechanical alignment

During the installation the muon chambers were mounted on the supporting walls with a precision of  $\sim 1$  mm centered on their nominal positions, calculated with respect to reference targets placed on top of each half station. The measured rotations were zero within the precision of 1 mrad. After chamber installation, the muon filters and the half stations were closed around the beam pipe. Since the muon filters could not be completely closed because of mechanical tolerances of the iron blocks, also the detector half stations were kept slightly open to avoid possible radiation damage. The opening of each half is  $\pm 5$  mm at M1 and increases with the  $z$  coordinate to preserve the projectivity of the muon chambers. The positions of the half stations with respect to the LHCb cavern reference were precisely surveyed using four reference targets on each side, and the values were stored in the geometry database that is used by the reconstruction program to define the absolute hit coordinates. The average  $x$  coordinate of the inner edges of the ten half stations, as measured by the survey, as a function of the  $z$  position is shown in figure 9.

### 5.1.2 Space alignment using tracks

An independent determination of the position of the muon detector elements can also be obtained analyzing the tracks reconstructed in the detector. This is extremely useful both to check the mechanical positioning of the chambers in the stations and to monitor the alignment of the muon stations after each opening and closure. By studying the residual distributions between the hit and the track coordinates over the different stations it is in principle possible to determine the detector misalignment and possibly mechanically correct it.

In case the track is defined only by the information of the muon detector, it is possible to study the relative alignment of the muon stations with respect to an arbitrary reference defined, for example, by fixing the position of two stations (*local alignment*). As a consequence, any additional degree of freedom of the muon system like global rotation, translations or shearing can only be determined aligning the muon detector by using the tracks reconstructed also by the tracking detectors of the experiment (*global alignment*).

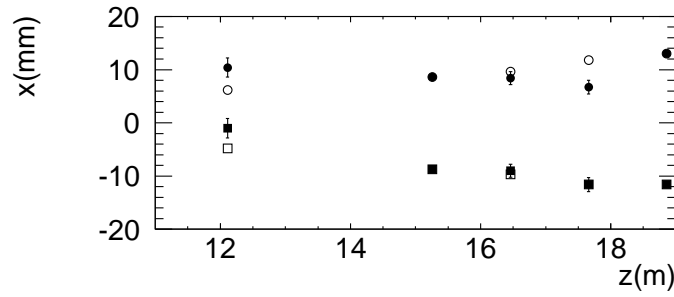
The analysis described here is focused on the study of the relative positions of the muon half stations since the statistics did not allow a precise study of single chamber alignment. To simplify the study further, only the most relevant degrees of freedom were considered, i.e. translations in  $x$  and  $y$  direction.

The local alignment of the muon half stations was studied with respect to the half stations of M2 and M5, that were used to define the reference. Only the tracks crossing the same side (C or A-side) of the stations were considered. The study was performed using two methods. In the *histogram* method the tracks were defined by the straight line joining the hits found in the two reference stations. The residuals on the remaining half stations were then calculated between the clusters center and the track fit position ( $r = x_{cluster} - x_{fit}$ ). The mean values represent the best estimates of the alignment parameters. With the *Kalman fit* method, instead, the alignment parameters were calculated iteratively by minimizing the total  $\chi^2$  of the track sample with respect to the alignment parameters until convergence is reached. While the first method is rather simple to analyze, the second one provides a more accurate track fit accounting for multiple scattering effects. The results of the two methods were found in agreement and the Kalman fit method was eventually used

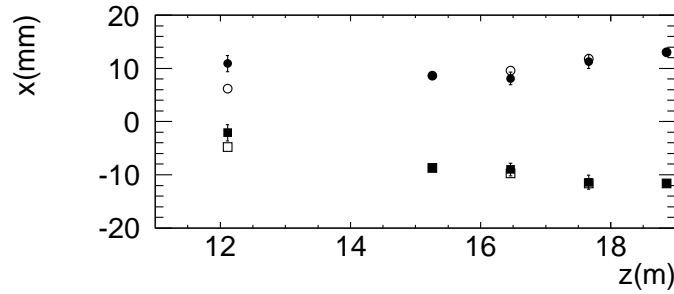
for the results in the following.

The systematic uncertainties, mainly due to the non uniform geometrical acceptance of the detector to cosmic ray tracks and to the rather poor granularity of the detector, were estimated with Monte Carlo data in the configuration of the aligned detector. They amount to about 1 mm along  $x$  and about 2 mm along  $y$  directions.

The study performed on a first data sample showed a significant displacement of the M4, A side, station along the  $x$  direction of  $\sim 5$  mm, far above the systematic errors of the method, as shown in figure 9(a). For this reason half station A of M4 was moved by  $\sim 4$  mm with respect to the other half stations M2A, M3A and M5A inside the common support to compensate the observed deviation. The analysis of data acquired after the displacement clearly shows the effectiveness of the correction, as one can see from figure 9(b). The results showed also misalignments along the



(a)



(b)

**Figure 9.** Average position along the  $x$  coordinate of the muon half stations before (a) and after (b) the displacement of station M4A (as described in section 5.1.2). The open circles (side A) and squares (side C) represent the survey measurements while the solid circles and squares are the positions obtained by the software local alignment with respect to the reference given by M2 and M5 stations. The errors are statistical only.

$x$  coordinate for M1 station, albeit with larger uncertainties. Since M1 halves can be easily moved independently of the other stations, it was decided to wait for more significant results with collision tracks before making adjustments.

The global alignment was performed relative to the OT detector. OT tracks were selected with a special setting of the track finding designed for cosmic rays and ignoring drift time information. Muon tracks matching the OT tracks were selected and analyzed with the Kalman fit iterative method to determine the alignment constants of the muon half stations. The reference was defined

assuming the first layer of the first OT station and the muon station M3 in their nominal position. The results are summarized in table 1. The results show an overall compatibility with the survey

**Table 1.** Misalignments  $\Delta x$  and  $\Delta y$  of muon half stations M1, M3, M4 and M5 with respect to the survey measurements calculated with the Kalman fit iterative method assuming the first layer of the first OT station and the muon station M2 in their nominal positions. The quoted errors are statistical only. The systematic errors amount to 1 and 2 mm along the  $x$  and  $y$  directions.

	C-side		A-side	
	$\Delta x$ (mm)	$\Delta y$ (mm)	$\Delta x$ (mm)	$\Delta y$ (mm)
M1	$1.8 \pm 0.2$	$-0.7 \pm 0.5$	$2.7 \pm 0.2$	$-1.8 \pm 0.5$
M2	—	—	—	—
M3	$1.1 \pm 0.2$	$-1.8 \pm 0.9$	$-0.7 \pm 0.2$	$-1.3 \pm 0.9$
M4	$1.3 \pm 0.7$	$-2.8 \pm 1.1$	$-1.6 \pm 0.7$	$-2.0 \pm 1.1$
M5	$1.1 \pm 0.8$	$-1.0 \pm 1.3$	$2.9 \pm 0.8$	$-2.9 \pm 1.3$

measurements. With tracks coming from the interaction point a more accurate determination of the alignment will be possible.

## 5.2 Time alignment

The muon trigger requires that particles are detected and assigned to the proper LHC bunch crossing in each of the five muon stations. The purpose of the time alignment is to adjust the delays of all detector channels in order to maximize the probability that the signals fall within the 25 ns gate around the correct bunch crossing.

The time alignment is achieved in a three step procedure, the first two of which do not rely on beam particles and are described in this paper. In the first step a pulser system sends test signals directly to the front-end input allowing to equalize the timing of the readout chain. In the second step, the cosmic ray tracks are used for a refinement of the detector internal alignment using physical signals. Its accuracy is limited, notably for the inner regions, by the available statistics and by the asynchronicity of the signals with the LHC clock. For this reason, the ultimate alignment will be achieved using particles from collision data, relying on the sharp arrival time of the beam bunches.

### 5.2.1 Pulser time alignment of the readout chain

The first step of the procedure was developed to time-align all readout channels making use of the Pulse Distribution Module (PDM) [10] and of the integrated timing facilities of the front-end (DIALOG chip) and off-detector (SYNC chip) electronics. The PDM received the LHC master clock and generated pulse signals corresponding to a pre-defined bunch crossing. This pulse was distributed to the front-end electronics through the Service Boards (SB) [11]. From the SB the pulse was injected into the front-end inputs and the related outputs following the normal path up to the ODE boards, where the signal time was measured by the SYNC TDC. In order to make optimal use of the delay ranges available at the DIALOG (52 ns in steps of 1.56 ns) and SYNC (175 ns in steps of 25 ns) level, the equalization proceeded in two steps. In the first step (fine time alignment),

the relative time of the pulse signal with respect to the 25 ns gate was measured by the SYNC TDC and the appropriate delays were calculated and loaded in the DIALOGs in order to center the time spectrum on the 25 ns LHC gate. In the second step (coarse time alignment), delays were applied to both the DIALOG and SYNC so that all the timing pulses were recorded in the same pre-defined 25 ns LHC gate.

The differences in the lengths of the cables bearing the pulse signals were compensated by appropriate corrections to the delays. Cable length values were precisely measured during the detector cabling phase and stored in a database. The uncertainty on these corrections limits the accuracy of the method to a few ns. Different chamber responses and particle time of flight also introduce misalignments that cannot be corrected by this procedure. Moreover, due to the complexity of the system and to the staged installation and commissioning of the detectors, in particular of the M1 station, the procedure was not fully achieved for the whole system before the cosmic ray data taking.

### 5.2.2 Time alignment using cosmic rays

In this step of the procedure, cosmic ray tracks were used to align the muon detector internally by comparing the measurements on the same track by different detector channels. With the reasonable assumption that all channels in a given FE board have the same timing, the misalignment of every FE board  $k$ , with respect to the other channels, was evaluated by averaging the residual

$$T_k = t_k - \frac{\sum_{i=1}^n t_i}{n} \quad (5.1)$$

over all tracks with a hit on FE board  $k$ . For each of the  $n$  measurements on a given track, the time  $t_i$  is obtained from the measured raw time  $t_R$  after correcting for the track non-projectivity as  $t = t_R + t_{PV} - t_\mu$ , where  $t_{PV}$  is the time of flight from the primary vertex and  $t_\mu$  is the actual time of flight of the cosmic muon from an arbitrary  $z$  reference value, computed according to the fitted track trajectory. The track direction is given unambiguously by the sign of the slope in the vertical plane, as shown in figure 8.

As described in section 1 there are three different readout configurations. In the regions where there is a one to one correspondence between the readout channel and the logical pad, the measurement is unambiguous. For the regions with double readout (M2/3 R1/2) the  $x$  and  $y$  time measurements were considered as independent and the time resolution was estimated separately for the two views. For the regions where the logical pads are obtained by crossing two  $x$  and  $y$  logical channels triggered by the same physical channel, the two measurements were averaged. In order to suppress the combinatorial background from the crossing of two unrelated logical channel hits, the two measurements were required to agree within 2 TDC bins (3.1 ns) for regions with single readout, and within 25 TDC bins (39 ns, more than 9 times the expected resolution) for regions with double readout.

Signals recorded in the first two and last two bins of the 16 bin range of the TDC were not used in this analysis, in order to remove the effect of an unwanted non-linear behavior of the TDC, which distorts the TDC spectra for signals falling near the borders of the LHC time gate. Even with this cut, some residual effect was left and was taken care of in the measurement of the time resolution,



as described in section 6.3.

For each FE board a correction was computed as  $\Delta T_k = -\alpha < T_k >$  and the procedure was iterated ( $\alpha = 0.8$  is a factor to damp possible oscillations) until the fraction of statistically significant corrections became negligible ( $< 1\%$ ). In case of hit clusters, all of them were used for the first three iterations, and only the first in time for the next ones, in order to suppress the effect of delayed cross-talk. The procedure converged after six iterations.

This calibration was limited by statistics for the inner regions. Though the average number of tracks recorded per FE board is over 50, the value is much smaller for the inner regions, notably for M1R1 (3.5 tracks/FE board on average). In order to avoid smearing the timing calibration with large statistical fluctuations, we applied the average correction of the corresponding region to the channels for which the computed correction was not significant.

The alignment with cosmic ray tracks allowed to identify and fix several problems of the pulse distribution cable chains. Systematic delays among stations of up to 10 ns were corrected, and smaller biases among sides or ODEs inside the same station were identified. The r.m.s of the statistically significant corrections amounts to 6.5 ns.

A second time alignment procedure using cosmic rays was developed independently, consisting in measuring the average channel delays with respect to the calorimeter trigger. In this alternative analysis, the channels, instead of being grouped by FE board, were divided in spatial regions containing chambers with the same characteristics. Those regions are large enough to provide statistically significant track samples but are not guaranteed to contain all channels with the same timing. Nevertheless the comparison of the two sets of constants shows an excellent agreement (85% correlation factor). The second procedure was used to compute the overall time shift needed to align the muon detector with the L0 trigger, while the previous stand-alone procedure was preferred for the relative alignment, in order not to be biased by possible imperfections of the calorimeter internal alignment, that was also being refined.

The stability of the alignment corrections was also checked by repeating the calibration with different cuts against the cross-talk and TDC non-linearity effects. No variations larger than 2 ns were observed.

## 6. Detector performance

### 6.1 Total efficiency

The efficiency calculation was performed with a re-run of the neural network based pattern recognition and track reconstruction, removing all hits of one station at the time. Then the number of tracks for which a hit was found inside a window of  $6 \times 4$  logical pads from the extrapolated point in that station divided by the total number of track candidates provided the efficiency values. The efficiencies obtained in this way were of the order of 85% on average, with the major source of inefficiency being the non hermeticity of the detector for tracks not coming from the interaction point. In order to get rid of this effect the efficiency was studied as a function of the angle  $\theta_{i,x(y)z}^P$  ( $i = 1, \dots, 5$ ) defined for each station  $M_i$  as the projected angle the track forms with the line connecting the hit with the interaction point (as illustrated in figure 10 for the yz projection). The efficiency was calculated as a function of  $\theta_{i,x(y)z}^P$  for the all stations, averaging the measurements

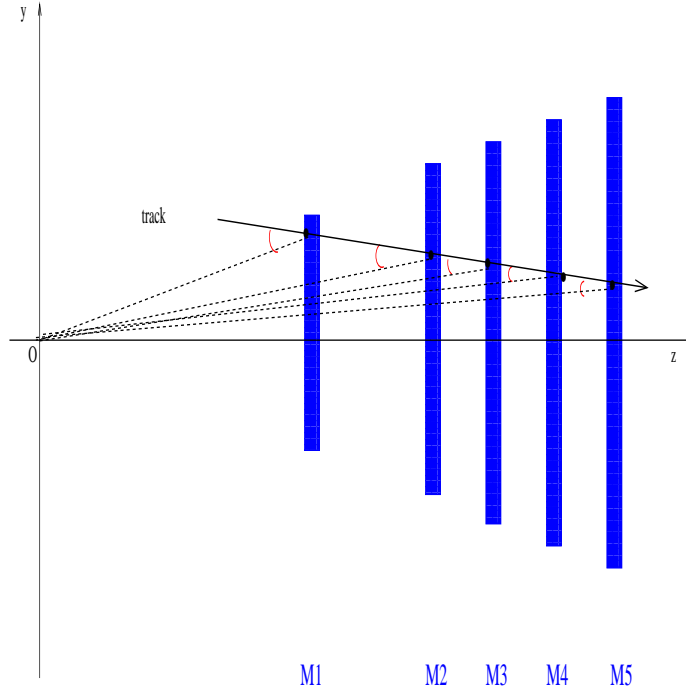


**Figure 10.** View (not to scale) of the LHCb muon detector on the  $yz$  plane. The projected angles  $\theta_{i,yz}^p$  for the five stations are shown. The drawing is not to scale.

of the four regions, to increase the statistical significance of the measurement. Since cosmic rays can be absorbed before reaching the outer stations M1 and M5 simulating chamber inefficiency, for the efficiency measurement of M1 and M5 only forward and backward tracks were used, respectively, and a fiducial region around the outer and inner regions of the detector was defined. The results for station M4 are shown in figure 11. The efficiency reaches a plateau value at small values of  $\tan(\theta_{i,yz}^p)$  for all stations while a flatter dependence on  $\tan(\theta_{i,xz}^p)$  is observed, explained by the smaller  $y$  size than  $x$  size of chambers, leading to a smaller hermeticity in the  $yz$  plane. Table 2 quotes the measured efficiencies for the five stations integrated over  $\tan(\theta_{i,yz}^p) < 0.06$  and  $\tan(\theta_{i,xz}^p) < 0.2$ . The latter cut was actually applied to define a fiducial region around zero angle also in the  $xz$  plane but, due to the quite flat dependence of the efficiency on  $\tan(\theta_{i,xz}^p)$ , has some degree of arbitrariness. Still the measured efficiencies are stable within 0.1 % with respect to the precise cut values.

**Table 2.** Total efficiency  $\varepsilon(\%)$  (in the wide gate) for tracks having  $\tan(\theta_{i,xz}^p) < 0.2$  and  $\tan(\theta_{i,yz}^p) < 0.06$  for the five stations of the LHCb muon detector.

	M1	M2	M3	M4	M5
$\varepsilon(\%)$	$98.8 \pm 0.4$	$99.7 \pm 0.1$	$99.9 \pm 0.1$	$99.8 \pm 0.1$	$99.8 \pm 0.1$

## 6.2 Cluster size

The track finding procedure of the muon trigger algorithm is based on logical pad signals which

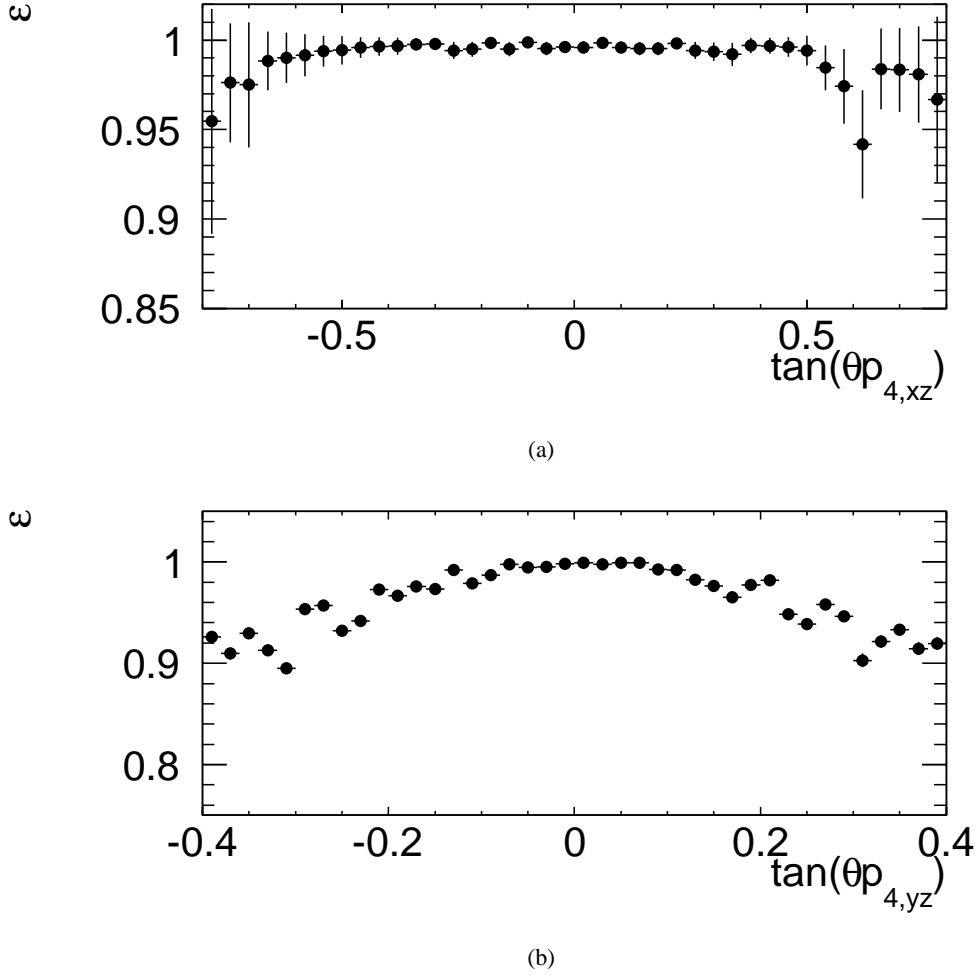


**Figure 11.** Efficiency  $\varepsilon$  as a function of  $\theta_{4,xz}^p$  (with  $\tan(\theta_{4,yz}^p) < 0.06$ ) (a) and  $\theta_{4,yz}^p$  (with  $\tan(\theta_{4,xz}^p) < 0.2$ ) (b) angle for station M4, as defined in figure 10.

are combined one per station to form five hit tracks, with the logical pads having a smaller size in  $x$  to measure the transverse momentum, as previously explained. To avoid spoiling the transverse momentum measurement and to limit the number of hit combinations (the trigger algorithm does not consider clusters) it is therefore important to minimize the cluster size (CS) along  $x$ , i.e. the number of adjacent logical pads along  $x$  fired by the same track. The cluster size is an intrinsic characteristic of a chamber, but it is also affected by track inclination, given the non negligible thickness of the multi-gap chambers. To distinguish between the two effects, the cluster size was measured as a function of the angle  $\psi_{xz}$  that the muon track makes with the perpendicular to the chamber.

Figure 12 shows the cluster size vs.  $\psi_{xz}$  for tracks with  $|\psi_{yz}| < 0.5$  rad for M2R3 (a) and M3R2 (b) chambers. In regions where the logical pads are smaller, a steeper dependence on  $\psi_{xz}$  is observed, as expected from the geometry.

The hits affecting the muon system performance in collision mode are only those occurring during the 25 ns LHC gate. Therefore our time integrated cluster size measurement is an over

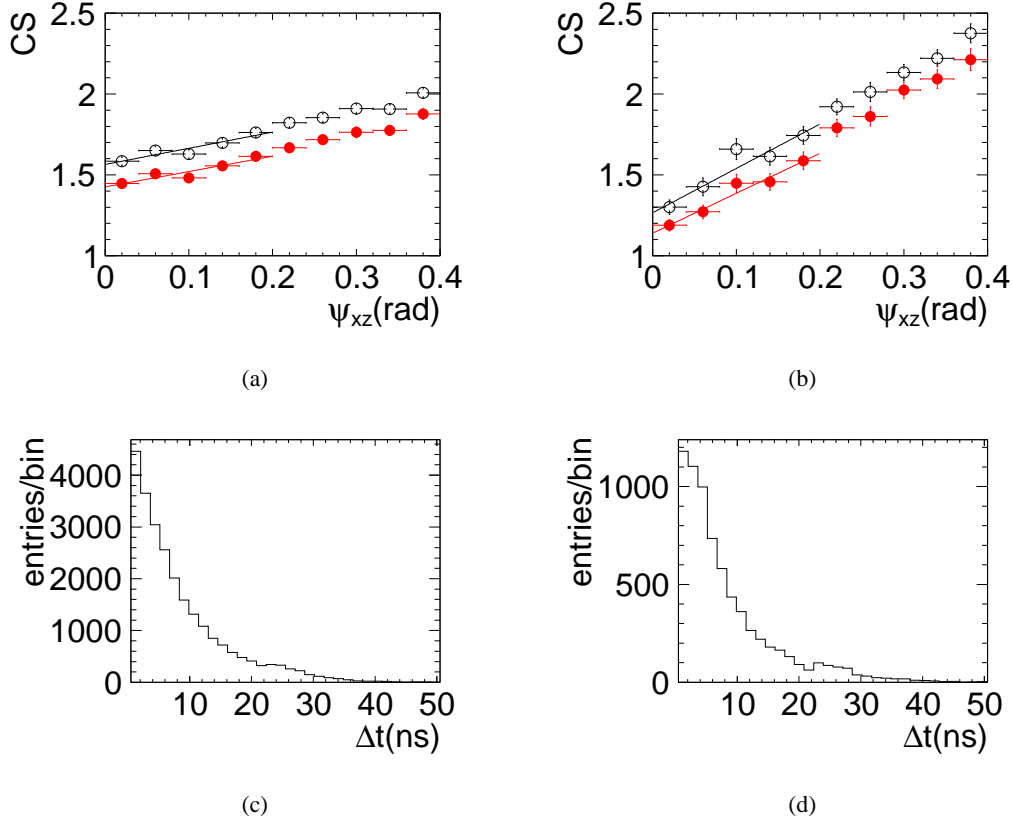
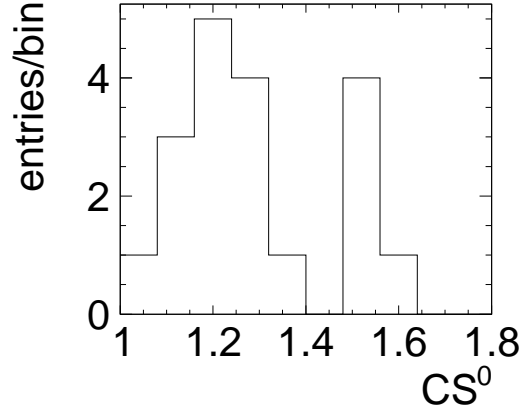
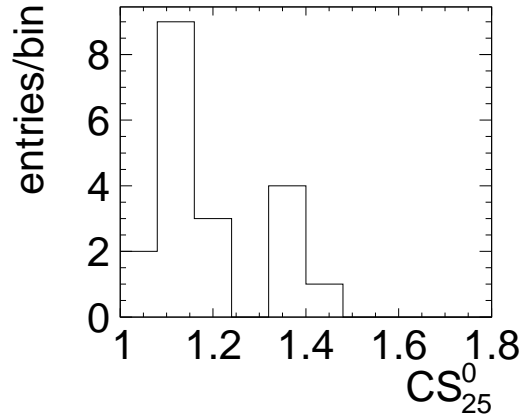


**Figure 12.** Average pad cluster size vs.  $\psi_{xz}$  for  $|\psi_{yz}| < 0.5$  rad in the wide gate (open circles) and in the 25 ns LHC gate (solid circles), for M2R3 (a) and M3R2 (b) chambers. Time ordered difference between the  $x$  logical channels forming the cluster and the one occurring first in time, in events with cluster size larger than one, for M2R3 (c) and M3R2 (d) chambers.

estimate of the effect. The cluster size in the 25 ns LHC gate,  $CS_{25}$  was derived by convoluting the measured time distribution of the main hit, as described in section 6.3, centred in the 25 ns LHC gate, with the experimental distribution of the time ordered difference between the  $x$  logical channels forming the cluster and the one occurring first in time, in events with cluster size larger than one, shown in figure 12 (c) for M2R3 and (d) for M3R2 chambers. Figure 12 shows the corrected cluster size vs.  $\psi_{xz}$  for  $|\psi_{yz}| < 0.5$  rad for M2R3 (a) and M3R2 (b) chambers. The first five open points of figure 12 were fitted with a straight line and the extrapolation of this line to zero angle,  $CS^0$ , was reported in figure 13(a), with one entry per chamber type. The typical uncertainty on  $CS^0$  is of the order 0.05 and is due to the uncertainty from the extrapolation. The first five solid points of the same figure were fitted with a straight line and the extrapolation of this line to zero angle,  $CS_{25}^0$ , was reported in figure 13(b), with one entry per chamber type. Most chamber types are well inside the specifications; for those stations and regions where  $CS_{25}^0$  is at the edges, there is a plan for the future running of the experiment to lower the high voltage value, which will bring the cluster size to even smaller values.



(a)



(b)

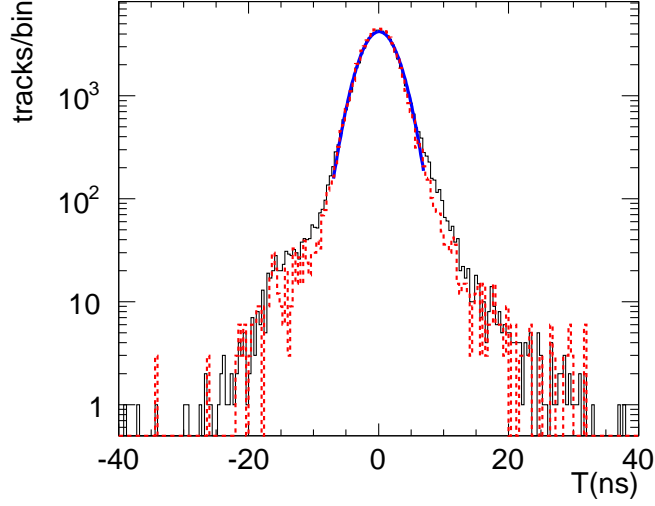
**Figure 13.** Logical pad cluster size at  $\psi_{xz} \rightarrow 0$  rad,  $CS^0$ , for tracks with  $\psi_{yz} < 0.5$  rad in an infinite time window  $CS$  (a) and in the 25 ns LHC gate  $CS_{25}^0$  (b). One entry per chamber type.

### 6.3 Time resolution

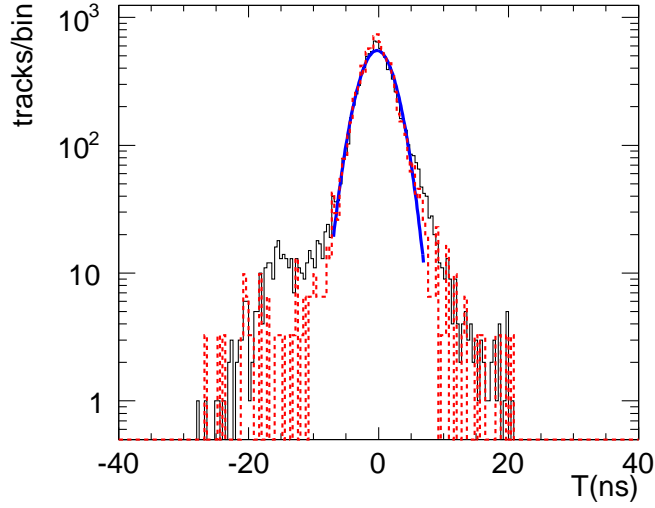
The detector time resolution was estimated for each region from the distributions of the time residual 5.1 after applying the corrections for time misalignments described in section 5.2. We used a data sample different, though acquired in similar conditions, from the one used for the time alignment, in order to avoid a bias on the time resolution from the over-training of the alignment.

The residual distributions exhibit some non gaussian tails. A detailed study was performed comparing regions characterized by a different readout method. An example is shown in figure 14. Tails are smaller for regions having the same physical signal read by two logical channels (for  $x$  and  $y$  views), where the coherence of the two measurements was required, as in figure 14(a). This suggests that tails are due to the TDC misbehavior at the 25 ns LHC gate borders and not to the intrinsic chamber response. As a further test of this hypothesis, the residuals were looked at, after selecting only forward tracks whose absolute time extrapolated at calorimeter, measured by the hits other than the one under scrutiny, is within  $\pm 6$  ns from the LHC gate center. For those tracks,

signals are expected to be more centered on the gate. The effect of this cut is shown on figure 14 for regions M5R4 and M3R2x. Since non-gaussian tails are mostly an artifact of the readout, the



(a)



(b)

**Figure 14.** Distribution of time residuals  $T$  for M5R4 (a) and M3R2  $x$  view (b) chambers. For M5R4 chambers the same physical signals is readout by two TDC channels for the  $x$  and  $y$  views, that were required to agree. For the M3R2 chambers there are two independent readouts for the two views. The dotted distribution is obtained after selecting tracks centered in the 25 ns LHC gate and is normalized to the same area of the full plot to show the effect on the tails.

resolution was eventually estimated from a gaussian fit performed on the core of the distribution of time residuals in region  $R$  for tracks with  $n = 5$  measurements:

$$s_{Rcore} = \frac{n}{n-1} \sqrt{\sigma_R^2(\text{resid}) - \frac{n-1}{n^2} \bar{\sigma}^2} \quad (6.1)$$

where  $\sigma_R(\text{resid})$  is the fit result and  $\bar{\sigma}$  is the average resolution estimated in the same way:

$$\bar{\sigma} = \sqrt{n/(n-1)} \sigma(\text{all residuals}).$$

Several systematic effects affecting the resolution measurement have been studied with the help

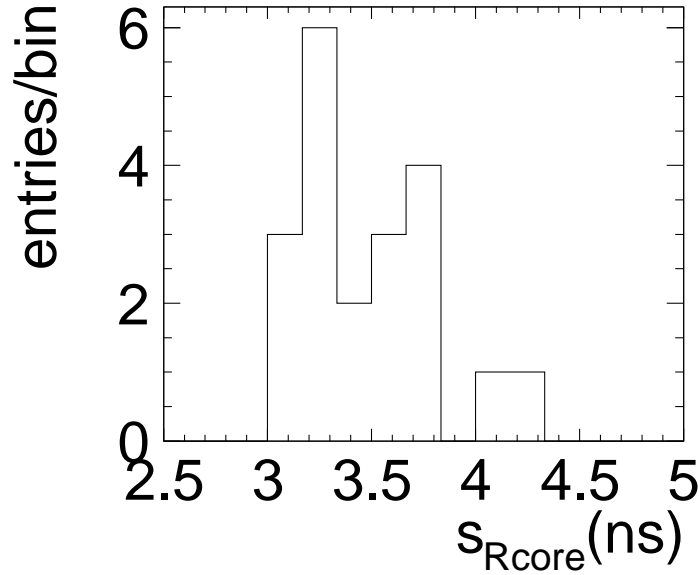


**Figure 15.** Resolution measurements  $s_{Rcore}$ , in ns, after correcting for the systematic effects. One entry corresponds to one chamber type; the chambers with double readout have two entries.

of a toy Monte Carlo, such as the removal of signals at the 2+2 border TDC bins, the selection of the first cluster hit in time, the residual time misalignments due to lack of statistics in some regions and the fit procedure.

The total systematic corrections turned out to be of the order of 0.1-0.2 ns and only for M1R1 and M2R2 amount to -0.7 and -0.6 ns, respectively. Figure 15, with one entry per chamber type, shows the final estimated resolution. For internal reference of the LHCb muon collaboration the results are also detailed in table 3, where the first column shows the  $s_{Rcore}$  resolution and the second column shows the final estimation after the systematic correction. The typical uncertainty on the single data point is of the order of 0.2 ns, including both statistical and systematic contributions.

It can be noticed that the time resolution results lie in the range between 3 and 4 ns; only two chamber types have time resolutions worse than 4 ns and it is due to residual time misalignment due to lack of statistics in the inner regions.

As discussed in section 3, with the cosmic data it was not possible to directly measure the 20 ns efficiency. Rather, from the measured values of time resolution and with the results of figure 6, an indirect estimate could be obtained, assuming the time resolution to be the only source of inefficiency, and showed that, apart from the triple-GEM M1R1 chambers, a 20ns efficiency above

**Table 3.** Resolution measurements, in ns, before ( $s_{Rcore}$ ) and after correcting for the systematic effects for the different chamber types.

chamber type	$s_{Rcore}$	final estimate
M1R1	$5.0 \pm 0.5$	$4.3 \pm 1.2$
M1R2	$4.0 \pm 0.4$	$3.4 \pm 0.6$
M1R3	$3.9 \pm 0.1$	$3.7 \pm 0.2$
M1R4	$4.0 \pm 0.1$	$3.8 \pm 0.2$
M2R1x	$3.0 \pm 0.2$	$3.1 \pm 0.3$
M2R1y	$3.0 \pm 0.2$	$3.1 \pm 0.3$
M2R2x	$3.0 \pm 0.1$	$3.2 \pm 0.2$
M2R2y	$3.0 \pm 0.1$	$3.2 \pm 0.2$
M2R3	$3.3 \pm 0.1$	$3.5 \pm 0.2$
M2R4	$3.3 \pm 0.1$	$3.3 \pm 0.1$
M3R1x	$3.4 \pm 0.2$	$3.6 \pm 0.3$
M3R1y	$3.2 \pm 0.2$	$3.4 \pm 0.3$
M3R2x	$3.0 \pm 0.1$	$3.2 \pm 0.2$
M3R2y	$3.0 \pm 0.1$	$3.2 \pm 0.2$
M3R3	$3.3 \pm 0.1$	$3.5 \pm 0.2$
M3R4	$3.1 \pm 0.1$	$3.1 \pm 0.1$
M4R1	$4.1 \pm 0.3$	$4.1 \pm 0.4$
M4R2	$3.6 \pm 0.1$	$3.7 \pm 0.2$
M4R3	$3.7 \pm 0.1$	$3.7 \pm 0.1$
M4R4	$3.2 \pm 0.1$	$3.3 \pm 0.2$
M5R1	$3.3 \pm 0.3$	$3.3 \pm 0.3$
M5R2	$3.4 \pm 0.2$	$3.5 \pm 0.3$
M5R3	$3.5 \pm 0.1$	$3.5 \pm 0.1$
M5R4	$3.3 \pm 0.1$	$3.3 \pm 0.1$

97.5% was archived.

A direct measurement of the 20 ns efficiency is going to be discussed in a future paper describing muon system performance with LHC beams.

## 7. Conclusions

A study of the LHCb muon system performance was presented, using cosmic ray data taken during the year 2009. The space and time alignment and the measurement of chamber total efficiency, time resolution and cluster size were discussed. The results confirm the expected detector performance.



## 8. Acknowledgments

The successful construction, installation and operation of the muon system would not have been possible without the technical support in each of the participating laboratories: we wish in particular to thank G. Paoluzzi, A. Salamon of INFN, Roma Tor Vergata, F. Maletta of INFN, Firenze, L. LaDelfa, D. Marras and M. Tuveri of INFN, Cagliari, W. Rinaldi and F. Iacoangeli of INFN, Roma.

We would like to thank the LHCb data acquisition team and the LHCb Calorimeter and Outer Tracker groups.

We also wish to thank the team of surveyors at CERN, in particular S. Berni and J.C. Gayde, for their important contribution to the detector alignment.

## References

- [1] The LHC Collaboration, *The LHCb Detector at the LHC*, 2008 *JINST* **3** S08005
- [2] W. Bonivento et al., *Development of the CARIOCA frontend chip for the LHCb muon detector*, *Nucl. Instrum. Methods A* **491** (2002) 233
- [3] S. Cadeddu, C. Deplano, A. Lai, *The DIALOG chip in the front-end electronics of the LHCb muon detector*, *IEEE Trans. Nucl. Sci.* **52** (2005) 2726
- [4] S. Cadeddu et al., *DIALOG and SYNC: A VLSI chip set for timing of the LHCb muon detector*, *IEEE Trans. Nucl. Sci.* **51** (2004) 1961
- [5] F. Legger, A. Bay, G. Haefeli, L. Locatelli, *TELL1 : development of a common readout board for LHCb*, *Nucl. Instrum. Methods Phys. Res. A* **535** (2004) 497
- [6] G. Martellotti et al., *Study of the performance of the LHCb MWPC with cosmic rays*, LHCb-PUB-2008-057
- [7] R. Veenhof, *Garfield; a simulation of gaseous detectors* Version 9 (4 Jul 2008)
- [8] A.P. Kashchuk, O.V. Levitskaya, *From noise to signal - a new approach to LHCb muon optimization*, LHCb-PUB-2009-018
- [9] G. Passaleva, *A recurrent neural network for track reconstruction in the LHCb Muon System*, *Nuclear Science Symposium Conference Record, NSS '08 IEEE* (2008) 867
- [10] V. Bocci et al., *Pulse Distribution Module (PDM) datasheet*, Muon Electronics Production Readiness Review Document - CERN
- [11] V. Bocci et al., *The services boards system for the LHCb muon detector*, *Nuclear Science Symposium Conference Record, 2007. NSS '07. IEEE* **3** (2007) 2134
- [12] T. Ruf, *Status of LHCb*, 10th LHCC Meeting open session, CERN, Feb.2010

